The Fourth IEEE RAS/EMBS International Conference
on Biomedical Robotics and Biomechatronics
Roma, Italy. June 24-27, 2012

Trade-offs in the implementation of rigid and intrinsically compliant actuators in biorobotic applications

Reyhan Zanis, Emilia Motoasca and Elena Lomonova

Abstract— **Actuators with intrinsic compliant elements are more and more being adopted in the biorobotics world. However, they also have a number of unfavorable characteristics such as bulkiness and a relatively high design complexity. Meanwhile, rigid actuators that are generally more compact and simple to implement are attractive for a number of applications. Yet, their inherent limitations in achieving a particular compliance characteristic might be in conflict with other biorobots design requirements. In this paper, we present experimental results to obtain more insights about the trade-offs in using three different types of single degree-of-freedom joint actuators, namely a geared rigid motor, a direct driven rigid motor and a variable stiffness actuator for biorobotic applications. Various aspects such as impact force behavior, stiffness range and manipulability as well as power consumption of the three actuator types are further investigated and compared in this paper.**

I. Introduction

Within the past decade, more and more robotics researchers worldwide began to consider biological features in their robot designs for various applications ranging from emulation of animal movements [14] to prosthetics [15]. One of the design consequences of these biorobots is that they need to have a soft actuation, implying a resemblance to the real biological counterparts and more importantly, the softness promotes a higher level of safety for themselves as well as for humans in their surroundings. The actuation softness of the biorobots can be introduced by

- implementation of a particular control algorithm (e.g. impedance control [1],[3],[6]), or
- incorporation of elastic elements at the robot's joint actuator [2],[3].

The first one is relatively simple to be performed as it requires a modification at a software level (control algorithm) and possibly an addition of a force/torque sensor at a hardware level. The second one is more difficult since a special actuation mechanism is required as both joint position and elasticity need to be controllable. Researchers have proposed a myriad of solutions (see [4] for a summary of the solutions) for achieving the intrinsic robotic joint elasticity.

In this paper, the trade-offs between the two mentioned ways of achieving the softness will be analyzed and discussed, by means of experimental verifications on a single link robot setup to evaluate their impact force behavior (which concerns the robot's actuator response to a sudden collision), stiffness/compliant range and manipulability as well as power consumption. A comparison criteria can be formulated based on the observed trade-offs and this can be used as a consideration in selecting an actuator type for biorobotic applications or even to synthesize novel actuators.

There are various actuators that can be used in biorobots: rigid ones, e.g. brushless DC motors, stepper motors [16] and intrinsically compliant ones, e.g. series elastic actuators [17], flexible pneumatic actuator [18]. However, only three types of actuators (two rigid and one intrinsically compliant) that are considered in this paper, namely a geared DC motor, a direct drive brushless AC motor and a variable stiffness actuator (VSA) [3]. The geared DC motor is advantageous due to its relatively small size and mass. Meanwhile, the direct drive motor, despite its large size due to a higher power rating for achieving a high torque level comparable to that of the geared DC motor, it does not exhibit the nonlinearities such as friction and backlash possessed by a gearbox [5], which could degrade its performance. On the other hand, the variable stiffness actuator has an intrinsic compliant elements which naturally react faster than control algorithms with inherent delays [1], [2] belonging to the geared DC motor and the brushless AC motor.

II. The actuators

A. Geared DC motor

The investigated brushed DC motor in this paper is MAXON RE 25 with a power rating of 20 W, integrated with a planetary gearbox having a ratio of 51:1. The motor has a theoretical (based on a datasheet calculation) maximum continuous torque of 1 Nm and a nominal speed of 200 rpm (21 rad/s). A simple impedance control in the form of a PD controller [6] is implemented to render rotor stiffness and damping characteristics, which is illustrated by the scheme shown in Fig. 1.

In Fig. 1, K and D are the rotor/joint stiffness and damping characteristics, respectively, θ_{ref} and θ are the reference and actual rotor position, respectively and T is the commanded motor torque, K_T is the motor torque constant and I is the current supplied to the motor. Note that with the assumption that the gearbox is stiff (which is true only to a certain extent), the measured θ is based on the division of the encoder signal (attached to the motor) by the gearbox ratio.

The resulting joint stiffness and damping which are generated by the controller are limited by the values of K and D which would lead the controlled system to instability and also inherent limitations of the motor, namely the maximum

This work was supported by SMAC Moving Coil Actuators.

R. Zanis, T. E. Motoasca, and E. A. Lomonova are with Electromechanics and Power Electronics Group, Department of Electrical Engineering, Eindhoven University of Technology, P.O. Box 513, 5600MB, Eindhoven, The Netherlands. Email: R.Zanis@tue.nl

allowed motor current (mainly due to thermal limits [11]) and gearbox backdrivability. In this context, backdrivability is the level of easiness to externally drive the gearbox's output shaft by introducing a torque, for instance through a manipulation performed by a human. The backdrivability is influenced by friction and inertia of the gear itself [7]. Due to the mentioned restrictions, the static stiffness (restoring torque to rotor deflection characteristic) range which is also a central issue in this paper is also limited, i.e. lower bounded by the backdrivability of the gearbox and upper bounded by the maximum allowed motor current, as illustrated in Fig. 2.

B. Direct drive brushless AC motor

In this paper, A Wittenstein MSSI-055H-045D brushless AC motor having a power rating of 300 W, with a maximum continous torque of approximately 0.7 Nm and a nominal speed of 4500 rpm (471 rad/s) is investigated. The impedance control scheme of in Fig. 1 is also implemented in the motor. The restrictions in achieving a certain joint stiffness and damping as previously mentioned apply for this motor as well. However, the lower bound as in Fig. 2 is generally very low due to the high backdrivability (therefore, the friction is low) of the direct drive mechanism.

C. Variable stiffness actuator

The variable stiffness actuator (VSA) is built based on the quasi antagonistic configuration [4],[3], using nonlinear springs that are constructed based on [8]. Two geared DC motors (see section II. A.) are used for controlling both joint stiffness and position. Fig. 3 shows the schematic of the VSA. As the rotor position of the stiffness motor θ_m changes, the two nonlinear springs are deflected, resulting in changes of both joint base position θ_j and stiffness. The joint link motor that is fixed on the joint base is able to control its link position θ_l independent of joint base position θ_j.

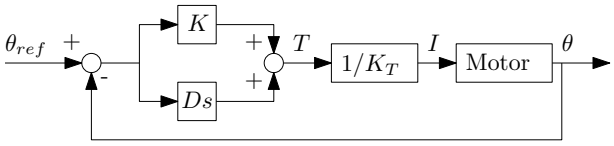

Fig. 1. Simple impedance control scheme.

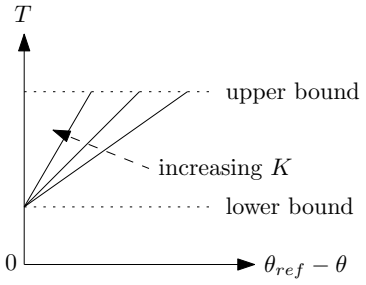

Fig. 2. Illustration of the lower and upper bound in the torque to deflection characteristic of the geared DC motor.

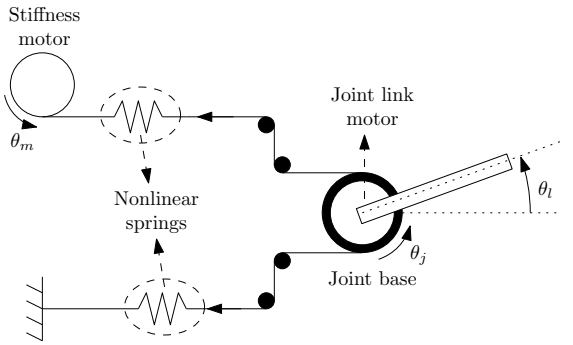

Fig. 3. The VSA which is based on the quasi antagonistic configuration.

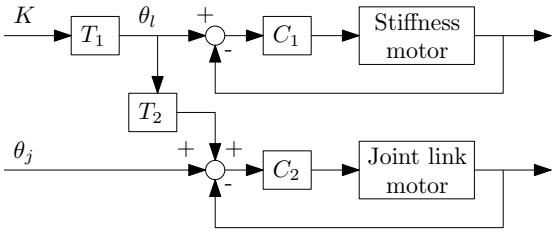

Fig. 4. Control scheme of the quasi antagonistic joint.

A control scheme for the quasi antagonistic joint is shown in Fig 4. Note that the joint stiffness K is controlled based on the motor angle through a static transformation T_1, which implies that its control accuracy is not guaranteed. The output of the T_1 block is also used to manipulate the joint link motor through the block T_2 as it is dependent on the stiffness motor position. The controllers C_1 and C_2 are tuned to have a sufficiently high bandwidth to ensure a high positioning accuracy and stiff behavior (note that the compliance is achieved through the springs).

Due to the particular nonlinear behavior of the spring's force versus deflection curve, the joint stiffness K range for the variable stiffness actuator is limited, which in the case of the investigated one is theoretically between 0.5 Nm/rad and 1.8 Nm/rad. As each of the nonlinear springs consist of linear springs, each with a minimum pull force to elongate it as well as maximum pull force that it can withstand, the lower and upper bounds as illustrated in Fig. 2 also apply for the actuator. In addition, these bounds are partly influenced by the dimensions of the springs.

III. Experiments

Two kinds of simple experiments involving biorobotic related tasks are performed for the three actuators. The first one is to investigate the impact force behavior of a link that is mounted on an actuator. The second one is performed to observe the ability of an actuator in changing its joint stiffness while the link is pushing against a certain object. Figure 5 shows the experimental setups of the three investigated actuators.

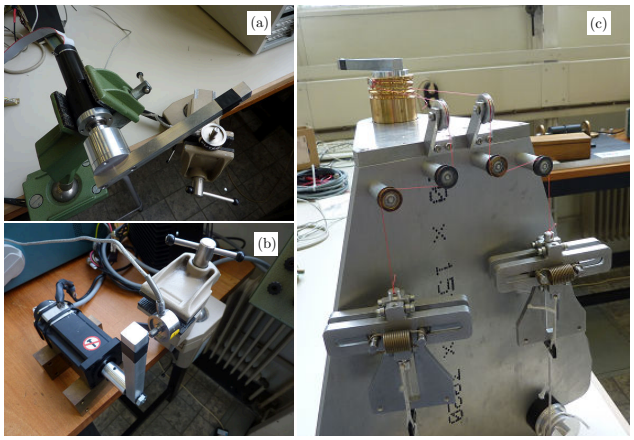

Fig. 5. Experimental setups: (a). geared motor, (b). direct drive motor, (c). Variable stiffness actuator.

A. *Impact force*

For the impact force test, a link is mounted on the rotor of each actuator. The actuator - link - force sensor (FUTEK LCM 300 load cell) configuration is shown in Fig. 6. In the figure, θ_{ref} indicates the motion setpoint which is designed based on the rigid body motion profile [9]. Certainly, the link will not be able to accomplish a full sweeping range of θ_{ref} as it is constrained by the force sensor. The rigid body motion profile, for which the maximum acceleration, velocity and position can be specified, that is used in the impact force experiment is depicted in Fig. 7. Furthermore, all of the actuators have the same values of joint stiffness K of 1.5 Nm/rad, while the joint damping D values (only for the rigid actuators) are selected to be close to zero, but resulting in a reasonable damped response. The resulting open-loop position control bandwidth of the two rigid actuators are in the range of 1 Hz - 10 Hz, while for the VSA is around 40 Hz. The hardware that is used for the control and data acquisition purposes of the experiments is a MATLAB-dSPACE system, which was operated with a sampling frequency of 10 kHz.

Fig. 8 shows the ideal impact behavior of the configuration shown in Fig. 6. The level of the peak impact force in Fig. 8 is influenced by the mass and velocity of the link, as illustrated by the basic physics concept of impulse imp

$$imp = F\Delta t = m\Delta v, \tag{1}$$

where F is the impact force, m is the mass of the moving object, t is time and v is the velocity of the object. Note that the for the investigated actuators, the mass m of the link may not include the rotor or other transmission systems on which it is mounted, as during the impact, the link is decoupled from the rest of its transmission due to the presence of a moderate level of stiffness [10]. After the impact, the force level increases as the link tries to follow the motion profile, with the force level depending on the value of joint stiffness K (which is defined in the controller for the case of rigid actuators).

Fig. 9 shows the impact behavior of the three different actuators. With respect to the peak level of the initial impact, the geared DC motor and the VSA have almost the same value of impact force of approximately 50 N, which is due to the same link effective mass (the link is likely to be decoupled from the gearbox during the impact). Meanwhile, the peak force level belonging to the direct drive motor is higher due to a higher link effective mass promoted by a highly stiff connection between the link and rotor.

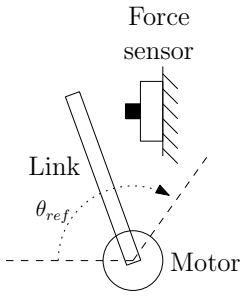

Fig. 6. Actuator - link - force sensor configuration for the impact force test.

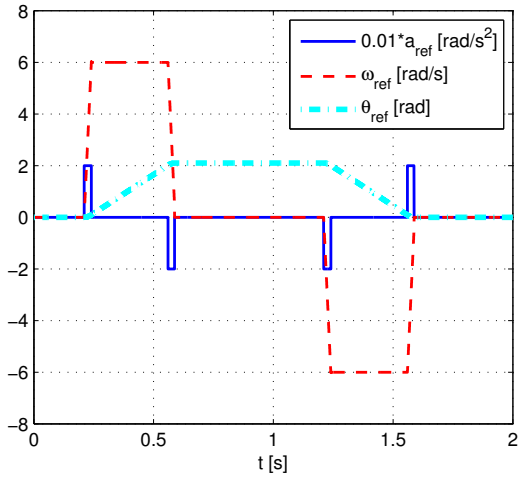

Fig. 7. Motion profile used in the impact force experiment.

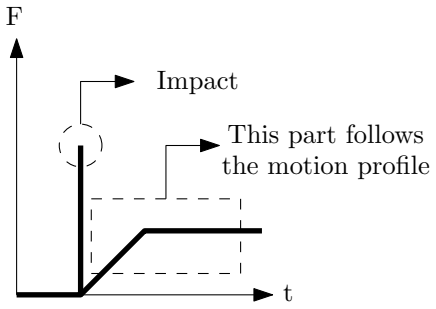

Fig. 8. Ideal impact force behavior.

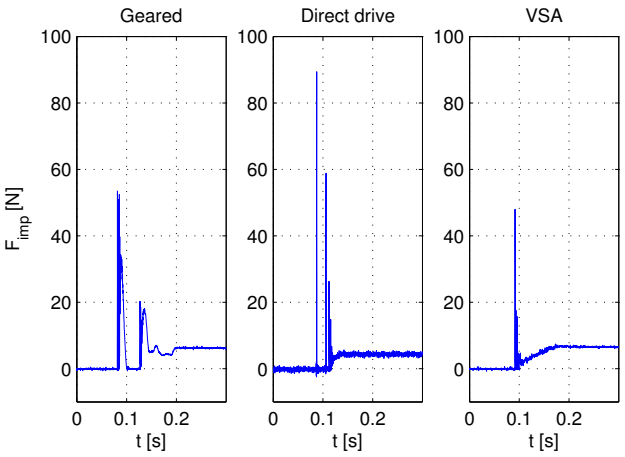

Fig. 9. Impact force behavior for the three actuators.

The behaviors after the impact for the three actuators are significantly different. As shown in Fig. 9, the after impact behavior of the VSA is the closest to the ideal one as shown in Fig. 8. This is possible since the energy that is transferred back to the actuator due to the impact is effectively (although not perfectly efficient) transferred to the real springs. Moreover, a sufficient amount of joint damping is present on the VSA, resulting in a relatively low force peaks after the initial impact force peak. Meanwhile, for the geared DC and the direct drive motors, different after impact behaviors are observed which are mainly due to the delay in the transfer of the impact energy to the control loop.

To further investigate the delay in the impact energy transfer to the control loop, an illustration based on the force balance in the control loop is presented in Fig. 10, where C is the controller, G represents the actuator/motor transfer function, F_{com} is the commanded force from the controller, F_{act} is the force sent to the actuator, F_{imp} is the impact force and F_{loss} is the force component that contribute to the losses inherent in the actuator (friction, damping, etc.). For the ideal case (no delays), the following equation holds

$$F_{com} - F_{act} - F_{loss} = F_{imp}. \tag{2}$$

Note that F_{loss} can only be estimated through the above force balance equation.

Fig. 11 highlights the after impact behavior of the geared and the direct drive motors as well as the corresponding force balance based on (2). For the case of the geared motor, there is an indication that the controller responds to the impact. However, it is not as expected, since the left hand side of (2) stays around zero indicating the impact energy is barely transferred to the controller. Moreover, multiple peaks with a subsequent long duration peak force as indicated by the dashed part of Fig. 12 indicates that the gearbox absorbs a large amount of the impact energy. Meanwhile, a controller response in the direct drive case can be observed from the subsequent (thus, delayed) peaks of the term $F_{com} - F_{act} - F_{loss}$ after the impact peaks. In addition, there is an apparent bouncing motion indicated by the multiple peaks, which could be caused by the deformation of the link itself.

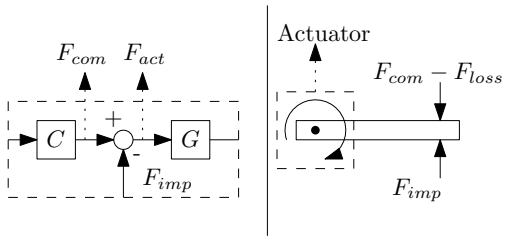

Fig. 10. Illustration of the force balance for the impact force test.

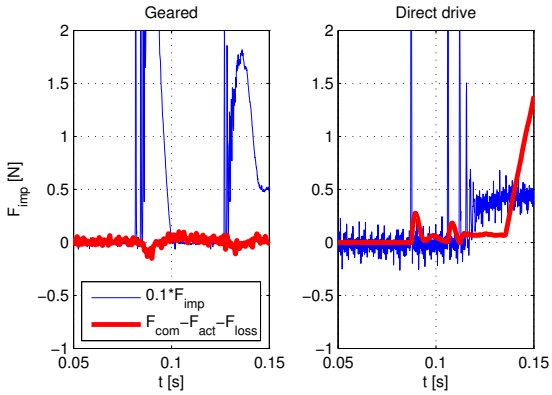

Fig. 11. Details of the impact force for the geared and direct driven cases.

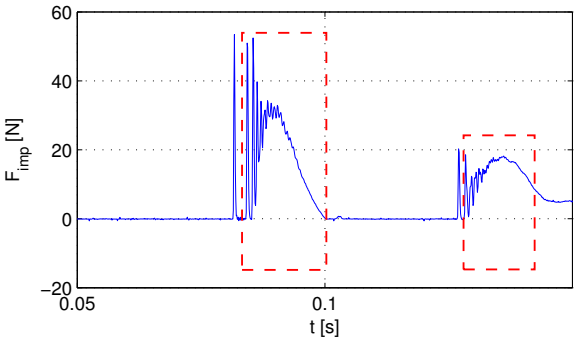

Fig. 12. Details of the impact force for the geared motor.

B. Static task with stiffness variation

This task concerns the manipulation of stiffness during a permanent contact of the link in Fig. 6 with the force sensor. Given that θ_{ref} in Fig. 6 is 120°, thus giving it a setpoint error of 30° during the permanent contact of the link, the reflected pushing force of the link can be calculated as follow

$$F_{push} = \frac{K \frac{30^\circ}{180^\circ} \pi}{l}, \tag{3}$$

where l is the distance between the center of the joint and the point on the link which would hit the force sensor. The measurement results of this task are presented in Fig. 13, in which the joint stiffness K is varied between 0.8 Nm/rad to 1.2 Nm/rad and the resulting pushing force F_{push} for the

ideal case and for the three actuators are shown. The results in Fig. 13 are summarized in the following points

- The direct drive motor has a response that is the closest to the ideal case. However, when K increases above 0.8 Nm/rad there is an apparent offset between the motor response and the ideal one, which is due to the maximum continuous current of the motor that has been reached.
- There is an apparent offset between the pushing force of the geared motor and of the ideal case over the range of K variation, this is due to the lowered efficiency in the presence of the gearbox. Moreover, it can also be seen that there is an inconsistent change in the resulting pushing force with respect to the K as indicated by the decreasing K value and a constant level of the pushing force due to the nonlinearities in the gearbox.
- For the VSA, the fact that the stiffness is in principle controlled in an open-loop manner results in even a larger discrepancy between the ideal pushing force and the real one. However, it has a better consistency in pushing force change compared to that of the geared motor.

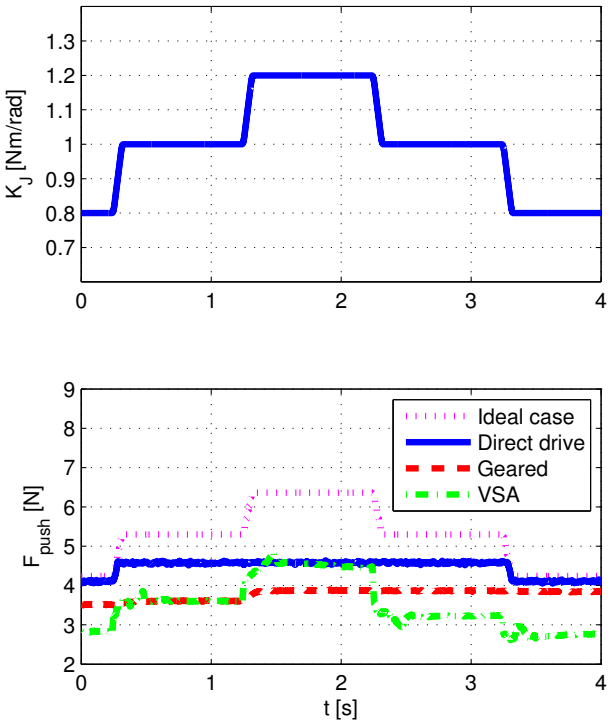

Fig. 13. Variation of the joint stiffness K (above) and its resulting pushing force (below).

C. Power consumption

The instantaneous input electrical power consumed by an electromagnetic actuator is given by the following equation

$$p_{in}(t) = V(t)I(t) = p_{EMloss}(t) + p_{mech}(t) = (i^2R + iL\frac{di}{dt}) + K_T\omega i, \quad (4)$$

where $V(t)$ is the instantaneous actuator terminal voltage, $I(t)$ is the instantaneous actuator current, R and L are the actuator winding(s) resistance and inductance, respectively and ω is the actuator rotor speed. In addition, the terms $p_{in}(t), p_{EMloss}(t)$ and $p_{mech}(t)$ denote the insantaneous input electrical power, electromagnetic losses (copper and iron) and total mechanical power (including friction losses) of the actuator, respectively.

Table I presents the RMS values of the input electrical power for the impact and stiffness variation tasks, including the electromagnetic losses (for the impact task only, as the other task involves no rotor motion). These RMS values are calculated over a time interval of 2 sec. and 5 sec. for the impact and the stiffness variations tasks, respectively. Apparently, the direct drive motor consumes the most electrical input power for the same tasks, which is due to a high electromagnetic losses. This is true since the direct drive motor is operated far below its operating range, implying a low efficiency. Meanwhile, it is not the case for the geared motor and the VSA since the gearbox alleviate the motor by bringing it to operate in the vicinity of its operating range.

TABLE I

RMS OF POWER CONSUMPTION FOR THE IMPACT AND THE STIFFNESS VARIATION TASKS.

Task	Geared	Dir. drive	VSA
Impact, P_{in}	1.63 W	6.6 W	2.2 W
Impact, P_{EMloss}	0.05 W	5.67 W	0.25 W
Stiffness variation, P_{in}	0.46 W	15.4 W	0.5 W

IV. DISCUSSION

Biorobots may appear in various configurations and size. In the design phase of biorobots, a designer may encounter a number of system specifications related to

- total size and weight,
- speed range,
- torque/force range,
- compliance/stiffness range and manipulability,
- high frequency impact behavior,
- electrical power consumption.

From the point of views of the mentioned aspects, each actuator discussed in this paper can be analyzed.

The use of a gearbox in the geared DC motor promotes a high torque, while keeping the achievable speed in the range of the general requirement of biorobots, which is normally much lower than the non-geared motor's nominal speed. This results in a compact size and a relatively lightweight actuator solution for biorobots. In terms of electrical power consumption, geared DC motors consume a relatively low

power as shown in Table I. The main problems of the geared DC motor arise from the nonlinearities of the gearbox that hinders the manipulation of compliance and absorb incoming disturbances instead of transferring it to the controller. The use of torque sensor alleviates the mentioned gearbox problems as presented in [3] and [12]. However, a designer may also want to avoid incorporating torque sensors for economic and simplicity reasons. For that reason, geared DC motors without torque sensor might suffice, at the cost of a poor contact/interaction ability.

Direct drive motors have normally a relatively high speed and low torque for robotic applications. As robots generally require a high torque, this results in the use of large and heavy direct drive motors. Therefore, such motors are better used for (bio)robotic applications that are stationary [13]. The stiffness of direct drive motors can be easily controlled without needing any torque/force feedback, as also shown in the experimental results in this paper, which is due to the very low friction. In addition, the brushless topology of the motor contributes in the reduction of the friction. In terms of electrical power consumption, direct drive motors are disadvantageous as discussed in the previous section. For that reason, such motors may not be suitable for mobile biorobotic applications that have limited energy storage capabilities.

The variable stiffness actuator (VSA), being the closest to their biological version by exploiting the use of intrinsic compliant elements result in a larger volume requirement and tend to become heavy. In addition, more than an actuator is needed. However, they have the best response to a high impact force as the impact energy is transferred to the compliant elements without being delayed, which is not the case for the impedance controlled geared and direct drive motors. Electrical power consumption of the VSA is still relatively low, despite the use of two motors. Therefore, mobile biorobotic applications with VSA could be feasible by considering a redesign of the compliant elements and the way the entire actuator system is configured, in order to make it more compact and lightweight.

V. Conclusions

TABLE II

Summary of the actuator's relevant aspects.

Aspect	Geared	Dir. drive	VSA
Size and weight	++	-	- -
Torque range	++	-	-
Stiffness manipulability	- -	++	+
Impact behavior	- -	+	++
Power consumption	++	- -	+

This paper discusses various performance related aspects of three different actuators for biorobotic applications, namely a geared DC motor, a direct drive motor and a variable stiffness actuator. The conducted experiments showed in detail the benefits and drawbacks of each actuator in performing biorobotics relevant tasks, such as response to a high impact force and manipulation of compliance/stiffness. Table II presents a summary of the actuator's relevant aspects which can be used as a basic guideline in selecting an actuator type for a biorobotic application or even to synthesize a novel actuator.

VI. Acknowledgements

The authors would like to thank SMAC Moving Coil Actuators for the funding of this research project.

References

[1] N. Hogan, "Impedance control: an approach to manipulation: Part I, II, and III," *Journal of Dynamic Systems, Measurement, and Control*, vol. 107, Mar. 1985.

[2] A. Bicchi and G. Tonietti, "Design, realization and control of soft robot arms for intrinsically safe interaction with humans," *Proceedings of the IARP/RAS Workshop on Technical Challenges for Dependable Robots in Human Environments*, pp. 79-87, 2002.

[3] A. Albu-Schaeffer, O. Eiberger, M. Grebenstein, S. Haddadin, C. Ott, T. Wimbock, S. Wolf and G. Hirzinger, "Soft robotics," *IEEE Robotics and Automation Magazine*, vol. 15, no. 3, pp. 20-30, Sept. 2008.

[4] O. Eiberger, S. Haddadin, M. Weis, A. Albu-Schaeffer, and G. Hirzinger, "On joint design with intrinsic variable compliance: derivation of the DLR QA-Joint," *ICRA 2010*, pp. 1687-1694, May 2010.

[5] J. Hollerbach, I. Hunter, J. Lang, S. Umans, R. Sepe, E. Vaaler and I. Garabieta, "The McGill/MIT direct drive motor project," *1993 IEEE International Conference on Robotics and Automation*, pp. 611-617, May 1993.

[6] N. Hogan and S. P. Buerger, "Impedance and interaction control," Robotics and Automation Handbook, CRC Press, pp. 19.1-19.24, 2005.

[7] T. Ishida and A. Takanishi, "A robot actuator development with high backdrivability," *2006 IEEE Conference on Robotics, Automation and Mechatronics*, pp. 1-6, June 2006.

[8] S. Migliore, E. Brown, and S. DeWeerth, "Biologically inspired joint stiffness control," *IEEE Int. Conf. on Robotics and Automation (ICRA 2005), Barcelona, Spain,* pp.4508-4513, 2005.

[9] P. Lambrechts, "Trajectory planning and feedforward design for electromechanical motion systems: version 2," Internal Report, Dynamics and Control Technology, Eindhoven University of Technology, Apr. 2003.

[10] S. Haddadin, A. Albu-Schaeffer, and G. Hirzinger, "Requirements for Safe Robots: Measurements, Analysis and New Insights," *The International Journal of Robotics Research*, 2009.

[11] J. M. Hollerbach, I. W. Hunter and J. A. Balantyne, "A comparative analysis of actuator technologies for robotics," *Robotics Review 2*, MIT Press, pp. 301-345, 1991.

[12] T. Wimboeck, M. Grebenstein, M. Chalon, W. Friedl, Ch. Ott, A. Albu-Schaeffer and G¿ Hirzinger, "From actively impedance controlled light weight robot hands to intrinsically compliant systems," ICRA 2011 workshop on manipulation under uncertainty, 2011.

[13] S. P. Buerger, J.J. Palazzolo, H. I. Krebs and N. Hogan, "Rehabilitation robotics: adapting robot behavior to suit patient needs and abilities," *Proceedings of the 2004 American Control Conference*, vol. 4, pp. 3293-3244, 2004.

[14] K. Berns, "Biological inspired walking machines," *Intelligent Autonomous Systems*, IOS Press, 2002.

[15] B. Dellon and Y. Matsuoka, "Prosthetics, exoskeletons, and rehabilitation [Grand Challenges of Robotics]," *IEEE Robotics and Automation Magazine*, vol. 14, no. 1, pp. 30-34, 2007.

[16] E. Dombre, G. Duchemin, P. Poignet and F. Pierrot, "Dermarob: a safe robot for reconstructive surgery," *IEEE Transations on Robotics and Automation*, vol. 19, no.5, pp. 876-884, 2003.

[17] G. A. Pratt and M. M. Williamson, "Series elastic actuators," *IEEE/RSJ International Conference on Intelligent Robots and Systems 95*, vol. 1, pp. 399-406, 1995.

[18] G. K. Klute, J. M. Czerniecki and B. Hannaford, "Artificial muscles: actuators for biorobotic systems," *The International Journal of Robotics Research*, vol. 21, no. 4, pp. 295-309, 2002.